Fast Maximum-Power-Point-Tracking for Photovoltaic Systems Based on P-V^2 Characteristic Curve and Its Stability Analysis

Ariyapuek, Monchai; Suwankawin, Surapong; Sangwongwanich, Somboon; Sangwongwanich, Ariya

Published in:
Proceeding of 2022 25th International Conference on Electrical Machines and Systems (ICEMS)

DOI (link to publication from Publisher):
10.1109/ICEMS56177.2022.9982888

Publication date:
2022

Document Version
Accepted author manuscript, peer reviewed version

Fast Maximum-Power-Point-Tracking for Photovoltaic Systems Based on P-V^2 Characteristic Curve and Its Stability Analysis

Monchai Ariyapuek
Dept. of Electrical Engineering
Chulalongkorn University
Bangkok, Thailand
6371029421@student.chula.ac.th

Surapong Suwankawin
Dept. of Electrical Engineering
Chulalongkorn University
Bangkok, Thailand
surapong.su@chula.ac.th

Somboon Sangwongwanich
Dept. of Electrical Engineering
Chulalongkorn University
Bangkok, Thailand
somboona@chula.ac.th

Ariya Sangwongwanich
Dept. of Energy Technology
Aalborg University
Aalborg, Denmark
ars@et.aau.dk

Abstract — To increase the tracking speed of the photovoltaic system (PV) for dynamic efficiency enhancement, a Maximum–Power–Point-Tracking (MPPT) method based on the P-V^2 curve is proposed. In contrast to the traditional design of MPPTs, it is demonstrated that the sampling frequency of MPPT can be increased to achieve an even faster dynamic than the settling time of the dc-voltage control loop as long as the closed-loop MPPT is still stable. Response time of the proposed P-V^2 based MPPT can be designed with a much faster dynamic than the conventional MPPT methods while its stability is guaranteed because i) adopting the squared PV voltage makes the dc-voltage control loop linear, and ii) the whole MPPT system conforms to the Lure's systems whose stability can be rigorously analyzed to obtain design guidelines for stable MPPT. Theoretical results are verified by simulation on Matlab/Simulink.

Keywords—Maximum power point tracking, dynamic response, P-V^2 curve, Lure's system, stability analysis.

I. Introduction

To maximize the energy harvesting from photovoltaic (PV) systems, maximum power point tracking (MPPT) is required [1]-[11]. Various MPPT algorithms proposed in the literature [1]-[2] use either the heuristic Perturb and Observer (P&O) searching algorithm or the feedback control configuration to attain the MPP condition [9]-[10]. So far, the P&O algorithm is more widely used than the feedback control approach since it offers simpler implementation in discrete-time domain and also due to the fact that the design of the feedback controller has not been systematically analyzed.

Based on the P-V curve in Fig. 1(a), two popular MPPT methods are the so-called P&O method and the Incremental Conductance (INC) method [3]-[8]. The two MPPT methods deploy basically the perturb and observe mechanism to track the MPP operating point. For a single-stage PV inverter shown in Fig. 2, the sampling time T_s of the MPPT must in general be set longer than the settling time of PV panel voltage or dc-link voltage control loop because the P&O algorithm must wait until the dc-link voltage control reaches the steady state before updating the voltage reference. The tracking speed of the MPPT is thus limited by the dc-link voltage control loop dynamic and may result in a deteriorated dynamic MPPT efficiency. In fact, it is possible to increase the tracking speed by sampling faster than the settling time of the dc-link voltage loop as shown as an example in Fig. 2 (the green line), but unstable MPPT can occur if the sampling rate is too fast (the blue line). The main obstacle which prevents the use of fast sampling rate is lack of stability analysis of the whole MPPT system.

On the other hand, the MPPT based on feedback control adjusts the PV panel voltage V_{pv} [9]-[10] through a PI controller. As such, the PV panel voltage is adjusted with a variable step size and oscillation around the MPP is alleviated. However, considering the non-linearity of the dc-link voltage control together with the MPPT based on feedback control, the closed-loop MPPT system becomes highly nonlinear and difficult to be analyzed or designed.

This paper aims to achieve fast MPPT dynamic with guaranteed stability by (i) introducing a new MPPT based on the characteristic curve between the power and the square of the PV panel voltage (P-V^2 curve) shown in Fig. 1(b) and (ii) deriving design guidelines from rigorous stability analysis of the closed-loop MPPT. The proposed MPPT algorithm and its theoretical analysis will be verified by simulation.

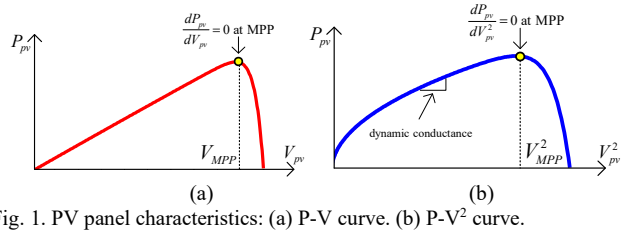

Fig. 1. PV panel characteristics: (a) P-V curve. (b) P-V^2 curve.

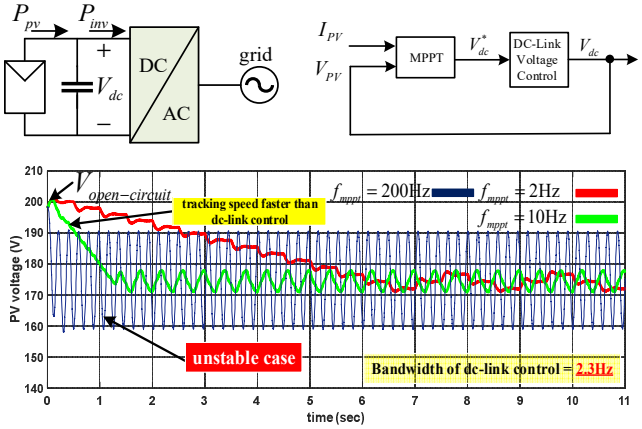

Fig. 2. Stability of P&O algorithm under various sampling rates when the settling time of the dc-link voltage control is about 100 ms.

II. Linear DC-Link Voltage Control and MPPT with Squared Voltage as a Control Variable

To allow rigorous stability analysis, first the nonlinearity due to the dc-link voltage control in the MPPT control loop as shown in Fig. 2 must first be removed. This is achieved by adopting the squared dc-link voltage as the controlled variable instead of the dc-link voltage itself, as explained in the following.

From the equivalent circuit in Fig. 2, dynamic equation of the capacitor voltage V_{dc} which is equal to V_{pv} is given by (1).

$$\frac{C}{2}\frac{dV_{dc}^2}{dt} = P_{pv} - P_{inv} \qquad (1)$$

978-1-6654-9302-4/22/$31.00 ©2022 IEEE

where C is the capacitance of the dc-link capacitor. Here, P_{inv} denotes the input power of the inverter which acts as the control input for the system, while the PV panel power P_{pv} is considered as an external disturbance.

Considering the dc-link voltage control, at present there are mainly two available configurations [14]. The first one is based on the control of the PV panel voltage V_{dc} directly as shown in Fig. 3(a). The main drawback of this configuration is that the closed-loop dc-link voltage control system is nonlinear.

To avoid this non-linearity, in this paper the squared dc-link voltage V_{dc}^2 is chosen as the control variable to make the voltage control loop linear as shown in Fig. 3(b). Consequently, since the dc-link voltage command is determined from the MPPT, it is desirable also that the MPPT should adopt the squared panel V_{PV}^2 or dc-link voltage V_{dc}^2 as the search or adjusted variable instead of the PV panel voltage V_{pv}. This naturally guides us to consider an alternative MPPT algorithm based on the P-V^2 characteristic of the PV panel rather than the P-V one as usually done. The overall MPPT system becomes as shown in Fig. 3(b), wherein the squared panel-voltage command V_{PV}^{2*} generated from the P-V^2 curve based MPPT is chosen as the set point for the dc-link voltage control loop. The linearity of the dc-link voltage control together with the proposed MPPT allow us to investigate the stability of the whole MPPT system based on the V_{PV}^2 variable as discussed in the sequel.

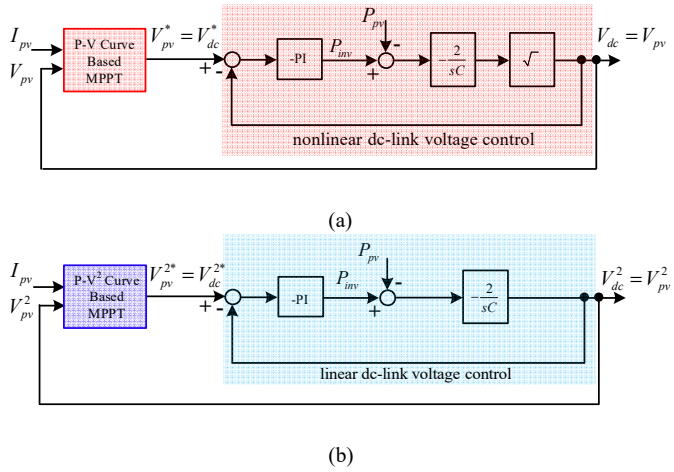

Fig. 3. DC-link voltage control. (a) V_{pv} as a command. (b) V_{pv}^2 as a command.

III. The New P-V^2 Curve Based MPPT and Comparison with Conventional P-V Curve Based MPPT

A. P-V Curve-Based P&O Method

For the P-V curve-based P&O method, the condition for MPP is given in (2).

$$D(V_{pv}) = \frac{dP_{pv}}{dV_{pv}} = 0 \ . \tag{2}$$

The derivative function $D(V_{pv})$ is shown as a graph of the PV panel voltage V_{pv} in Fig. 4 (the solid line). The MPPT algorithm attains the MPP by searching for the zero-crossing point of the $D(V_{pv})$ curve through the P&O algorithm. The dynamic behavior of the P&O based MPPT method is thus governed by the characteristic curve $D(V_{pv})$ of the PV panel.

B. Incremental Conductance Method

According to the INC method, the MPP condition (2) of the P-V curve is manipulated to obtain the condition (3).

$$C(V_{pv}) = \frac{I_{pv}}{V_{pv}} + \frac{dI_{pv}}{dV_{pv}} = 0 \tag{3}$$

Similar to the P&O method, the INC method attains the MPP by searching for the zero-crossing point of the curve $C(V_{pv})$ shown in Fig. 4 as a dashed line. Dynamic behavior of the INC MPPT method is determined by the characteristic curve $C(V_{pv})$, which is clearly different from the curve $D(V_{pv})$ of the P&O method. Although the signs of $C(V_{pv})$ and $D(V_{pv})$ with respect to the PV panel voltage around the MPP are the same, dynamic behaviors become different when both the magnitude and sign of $C(V_{pv})$ or $D(V_{pv})$ are used in the searching algorithm, as in the MPPT based on feedback control or the MPPT with variable step-size [8].

C. The Proposed P-V^2 Curve-Based MPPT

In the proposed MPPT method, instead of the P-V curve, the P-V^2 curve shown in Fig. 1 (b) is considered. From this

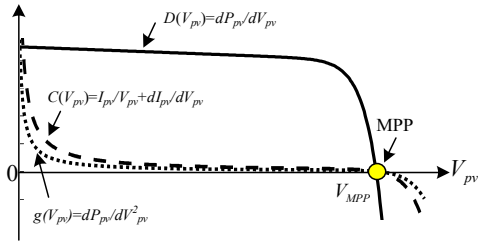

Fig. 4. Characteristic curves of the P&O, the INC, and the proposed methods. $D(V_{pv})$: solid line, $C(V_{pv})$: dashed line, and $g(V_{pv})$: dotted line.

P-V^2 curve, an alternative definition of instantaneous conductance G can be defined as shown in (4).

$$G = P_{pv} / V_{pv}^2 . \tag{4}$$

Also, the dynamic conductance g can be defined from the slope of the tangent to the P-V^2 curve as

$$g = \frac{dP_{pv}}{dV_{pv}^2} \ . \tag{5}$$

It can be seen from the P-V^2 curve in Fig. 1 (b) that at the MPP (V_{pv}=V_{MPP}) the so-defined dynamic conductance g must be zero, i.e.,

$$g(V_{pv}) = 0 \quad \text{at } V_{pv} = V_{MPP} \ . \tag{6}$$

The concept of the P-V^2 curve based MPPT is simply to search for the operating voltage under which the dynamic conductance g becomes zero. For comparison, the dynamic conductance g which characterizes the dynamic behavior of the proposed MPPT is plotted as a function of the PV panel voltage V_{pv} (the dotted line) in Fig. 4.

D. Equivalence between the INC method and the P-V^2 curve-based MPPT method

Equivalence between the P-V^2 curve based MPPT and the INC method is proven as follows. From (5) and (3), the following relationship can be derived.

$$g(V_{pv}) = \frac{dP_{pv}}{dV_{pv}^2} = \frac{dP_{pv}/dV_{pv}}{dV_{pv}^2/dV_{pv}} = \frac{1}{2V_{pv}}\frac{dP_{pv}}{dV_{pv}} = \frac{1}{2}C(V_{pv}) . \tag{7}$$

The relation (7) reveals that except for the coefficient ½, the curve $C(V_{pv})$ represents essentially the dynamic

conductance g defined from the P-V^2 curve. Even though the INC method is originally derived from the P-V curve, it is more appropriate to conclude from Fig. 4 and (7) that the INC method is in fact characterized by the P-V^2 curve not the P-V curve as usually understood. Comparison of the three MPPT algorithms is summarized in TABLE I.

The proposed P-V^2 curve based MPPT gives the same static and dynamic behavior as that of the INC method, but with simpler searching condition (6) compared to (3). The major difference between the INC and the proposed MPPT is the adopted search or control variable. Since the proposed MPPT algorithm searches for the MPP by varying the squared voltage V_{PV}^2, hereafter the dynamic conductance g in (5) and the MPP condition in (6) will be expressed as functions of the squared voltage (V_{PV}^2) as shown in (8) and (9). The dynamic behavior of the P-V^2 curve based MPPT under various irradiation conditions can be investigated by using the characteristic curves redrawn in Fig. 5.

Dynamic conductance: $$g(V_{pv}^2)=\frac{dP_{pv}}{dV_{pv}^2}. \quad (8)$$

MPP condition: $$g(V_{pv}^2)=0 \quad \text{at } V_{pv}^2=V_{MPP}^2. \quad (9)$$

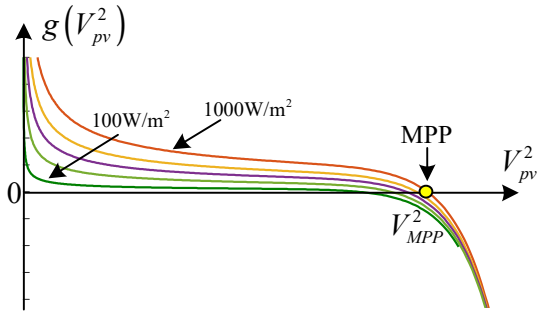

Fig. 5. Dynamic conductance g as a function of V^2_{pv} under various irradiation levels.

TABLE I. COMPARISON AMONG THREE MPPT METHODS

Methods	Error signal	Search variable	Condition at MPP
P&O	$D(V_{pv})=dP_{pv}/dV_{pv}$ Slope of P-V curve	V_{pv}	$D(V_{pv})=0$
INC	$C(V_{pv})=I_{pv}/V_{pv}+dI_{pv}/dV_{pv}$ Slope of P-V^2 curve (x2)	V_{pv}	$C(V_{pv})=0$
Proposed Method	$g(V_{pv}^2)=dP_{pv}/dV_{pv}^2$ Slope of P-V^2 curve	V_{pv}^2	$g(V_{pv}^2)=0$

IV. STABILITY ANALYSIS OF THE P-V^2 CURVE BASED MPPT

A. P-V^2 curve based MPPT using P&O algorithm

The P-V^2 curve-based MPPT method can use any extremum-seeking algorithm to search for the MPP. First, the perturb and observe algorithm shown in Fig. 6 is considered, by which the squared voltage V_{PV}^2 is perturbed with a step size Δ_{V2}, and the change in P_{pv} is observed. The dynamic conductance g in (8) is subsequently evaluated, and only its sign is used to update the squared voltage command V_{PV}^{2*}. This procedure is simpler than the equivalent INC method. The corresponding closed-loop block diagram of the INC method can be derived as depicted in Fig. 7, where $G_{dc}(s)$ is the transfer functions of the dc-link voltage control loop. As can be seen from Fig. 7, both the feedforward and feedback parts contain nonlinear elements make analysis difficult.

B. P-V^2 curve based MPPT using feedback control

The P-V^2 curve-based MPPT can also be implemented in a feedback control manner as shown in Fig. 8. In this scheme, the MPPT part (blue box in Fig. 8) is usually the PI controller. This scheme allows continuous tracking of the MPP without having to wait for the settling of the dc-link voltage control. The tracking speed is expected to improve as compared to the P&O algorithm. However, the non-linearity of the feedback path in Fig. 8 still obscures further stability analysis.

For comparison, block diagram of the conventional INC method is shown in Fig. 9. It is noted that all the three blocks are nonlinear, and the reference signal I_{pv}/V_{pv} is time-varying and depends on V_{dc} as well. Therefore, the stability analysis is much more complicated as compared to those of Figs. 7 and 8.

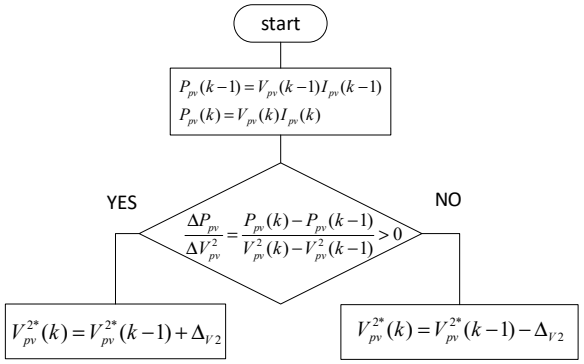

Fig. 6. The P-V^2 curve-based MPPT using P&O algorithm.

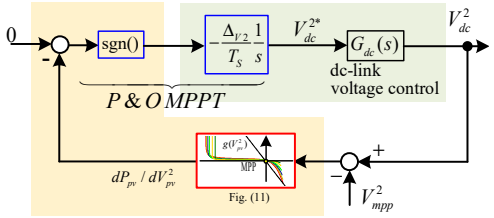

Fig. 7. Block diagram of the P-V^2 curve-based MPPT using P&O algorithm.

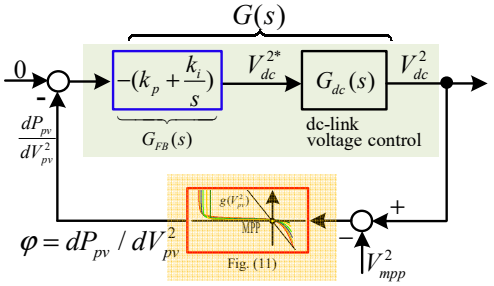

Fig. 8. Block diagram of the P-V^2 curve-based MPPT using feedback control.

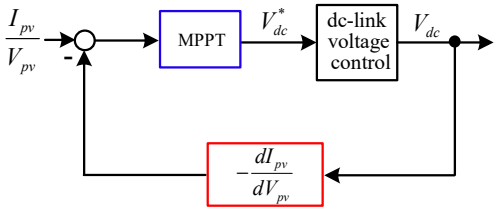

Fig. 9. Block diagram of the conventional INC method.

C. Stability analysis of the P-V^2 curve based MPPT

Although the closed-loop MPPT systems shown in Figs. 7 and 8 contains a non-linear element, it appears only in the feedback path owing to the linearity of the dc-link voltage control. Furthermore, it can be seen from Fig. 5 that the non-linear feedback path corresponds to the dynamic conductance function g which satisfies a sector-bounded condition around its MPP. As such, the closed-loop structure of Figs. 7 and 8 belongs, in fact, to the well-known Lure's system as shown in Fig. 10 with $y = V_{PV}^2$, whose feedforward (green) block $G(s)$ is linear, and feedback (orange) block $\varphi(y,t)$ is a sector-bounded non-linear time-varying function. Therefore, the absolute stability conditions for the Lure's systems [13] can be applied to derive the sufficient conditions for the closed-loop MPPT systems to be stable as follows.

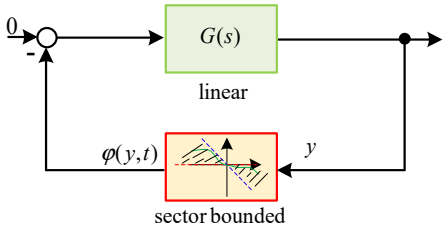

Fig. 10. The standard form of Lure's systems.

Stability condition from the circle criterion:

$$\mathrm{Re}\,G(j\omega) - 1/k_2 < 0 \text{ where } -k_2 \le \varphi(V_{PV}^2)/V_{PV}^2 \le 0. \quad (10)$$

$G(s)$ is the product between the transfer functions of the MPPT $G_{FB}(s)$ and the dc-link voltage control loop $G_{dc}(s)$, while k_2 is determined from the sector boundedness of the dynamic conductance function $\varphi = g = dP_{pv}/dV_{pv}^2$ (Fig. 5). This means that the Nyquist plot of the transfer function $G(s)$ must lie entirely on the lef-hand side of the $1/k_2$ line. To use the condition (10) to check the stability of the designed MPPT, the linear transfer function $G(s)$ must be computed.

From Fig. 3(b), the closed-loop transfer function $G_{dc}(s)$ of the dc-link voltage control can be expressed as in (11).

$$V_{dc}^2(s) = G_{dc}(s)V_{dc}^{2*}$$
$$G_{dc}(s) = \frac{k_{p-dc}s + k_{i-dc}}{s^2C/2 + sk_{p-dc} + k_{i-dc}} \quad (11)$$

where $k_{p\text{-}dc}$ and $k_{i\text{-}dc}$ are the proportional and integral gains of the dc-link voltage control, and C is equal to 820uF. In this paper, the $k_{p\text{-}dc}$ and $k_{i\text{-}dc}$ are selected as 0.024 W/V^2 and 0.01 W/V^2, respectively, to achieve a settling time of the dc-link voltage control loop around 100 ms. As a result, the feedforward transfer function $G(s)$ becomes as shown in (12).

$$G(s) = \underbrace{\left(\frac{k_p + sk_i}{s}\right)}_{G_{FB}(s)}\underbrace{\left(\frac{k_{p-dc}s + k_{i-dc}}{s^2C/2 + sk_{p-dc} + k_{i-dc}}\right)}_{G_{dc}(s)}$$
$$= \frac{-(48s^2 + 107540s + 44800)}{8.2\times10^{-7}s^4 + 820\times10^{-6}s^3 + 0.048s^2 + 0.02s} \quad (12)$$

where k_p and k_i are the proportional and integral gains, of P-V^2 curve-based MPPT, respectively. In this paper, the proportional and integral gains of the MPPT are set to 1000 and 2.24 x10^6 respectively to obtain a response time around 0.2 sec.

Next, before applying the condition (10), the value of k_2 which defines the sector boundedness should be determined. Fig. 11 is the graph of the dynamic conductance curve $g(V_{pv}^2)$ at various irradiations. The curves are calculated from the PV panel characteristic at 1000W/m^2 irradiation, whose open-circuit voltage and short-circuit current are 200V and 3.3A, the MPP voltage is 175V, and the rated power is 545W. From these dynamic conductance curves $g(V_{pv}^2)$, the parameters for the sector boundedness are determined as k_1=0, k_2=-19x10^{-6} as shown in Fig. 11.

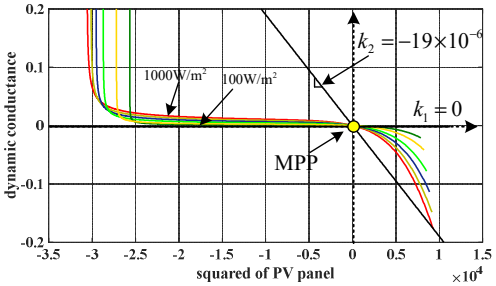

Fig. 11. Dynamic conductance under various irradiation levels with sector boundedness k_1=0 and k_2=-19x10^{-6}.

We can now investigate the stability of the designed MPPT by plotting the Nyquist plot of the transfers function G(s) as depicted Fig. 12. The trajectory of the Nyquist plot lies entirely on the left-hand side of the $1/k_2$ line and does not encircle the $1/k_2$ point. Therefore, it is concluded that the designed closed-loop MPPT satisfies the condition (10) and has an absolute stability.

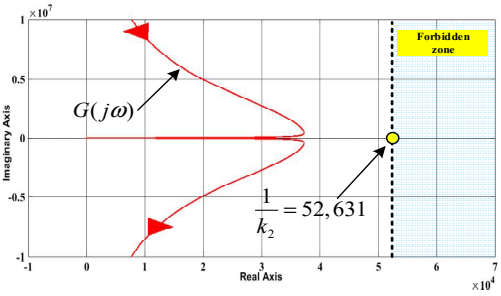

Fig. 12. Nyquist plot $G(s)$ of the designed MPPT.

V. Simulation Results

To investigate the correctness of theory and the feasibility of the proposed MPPT method, simulation using Matlab/Simulink is done on a single-stage 3-level PV inverter shown in Fig. 13. Two PV strings are connected to the upper and lower dc buses of the 3-level PV inverter. The proposed MPPT is performed on both strings separately. The PWM modulation scheme is given in [15]. The parameters of the PV string are the same as those used in the Fig. 11.

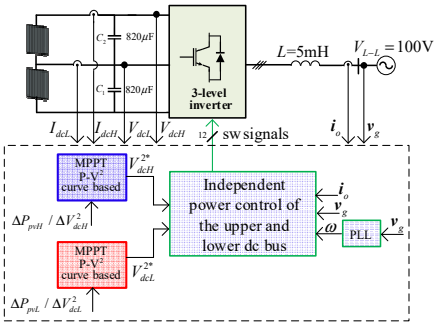

Fig. 13. Block diagram of simulation set up.

To validate the effectiveness of the proposed MPPT, the initial PV voltage is set at 190 V with the MPP voltage at 175 V. The simulation results are shown in Fig. 14. From Fig. 14 (a), the squared voltages (V_{dcH}^2, V_{dcL}^2) are adjusted correctly toward the MPP at 175^2 V^2 within 0.2 sec, and the generated power from each string reaches P_{pvH},=P_{pvL}=545W. The response time to the MPP is approximately 0.2 sec which corresponds closely to the analysis and design in the previous section. The trajectory of the tracking is illustrated on the P-V^2 plane in Fig. 14(b). From this simulation results, it is confirmed that the proposed P-V^2 curve-based MPPT system is stable as predicted from the circle criterion of Nyquist plot in Fig. 12 and works correctly as designed.

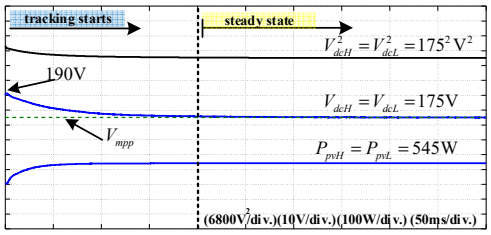

(a)

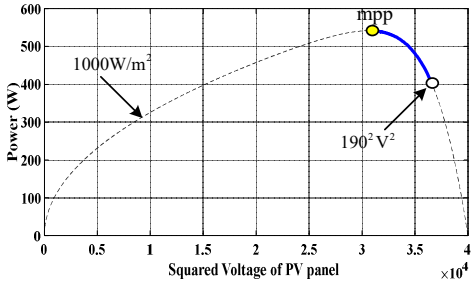

(b)

Fig. 14. Simulation results with the proposed P-V^2 curve-based MPPT using feedback control. (a) Transient response and convergence behavior. (b) Trajectory on the P-V^2curve.

For comparison, the simulation results with the P-V^2 curve-based MPPT using P&O algorithm instead of the feedback control (Fig. 6) are shown in Fig. 15. Considering the response time of the dc-link voltage control (100 ms), the sampling rate of P&O algorithm is set at 10 Hz (i.e., sampling time=100 ms) with the step size of the squared voltage Δ_{V2} of 600 [V^2]. Fig. 15 indicates that the response time of the P&O algorithm is much slower than the feedback control one.

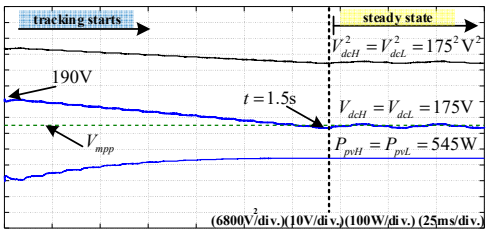

Fig. 15. Transient response and convergence behavior with the P-V^2 curve-based MPPT using P&O algorithm.

To demonstrate the dynamic performance of the proposed P-V^2 curve-based MPPT, the irradiance I_{rr} is now increased from 500 W/m^2 to 1000 W/m^2 with the ramp rate of 100 W/m^2/sec as shown in Fig. 16. The simulation results in Fig. 16 indicate that the MPPT can tracks the changing MPP very well as can be seen from the waveform of the dc-link voltage and from the trajectory in the P-V^2 plane. Moreover, despite of the changing irradiance, the MPPT is still stable and operates correctly without wrong tracking direction. This confirms the good dynamic performance.

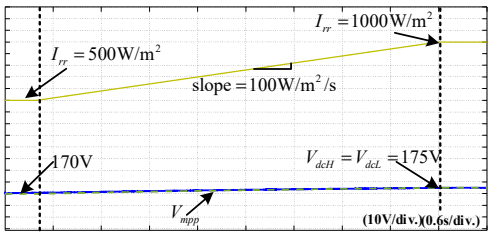

(a)

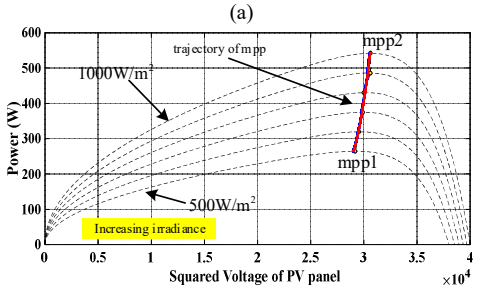

(b)

Fig. 16. Simulation results with the proposed P-V^2 curve-based MPPT using feedback control under dynamic irradiance condition. (a) Transient response and convergence behavior. (b) Trajectory on the P-V^2curve.

Similarly, the simulation results under the same conditions of Fig. 16 but with P&O algorithm are shown in Fig. 17. Compared to Fig. 16, it is seen that the P&O algorithm tracks in the wrong direction during transient because the irradiance changes so fast that the MPPT cannot differentiate the change of power whether it is due to the P-V characteristic or the changing irradiance. The dynamic performance is thus inferior to the proposed MPPT with feedback control.

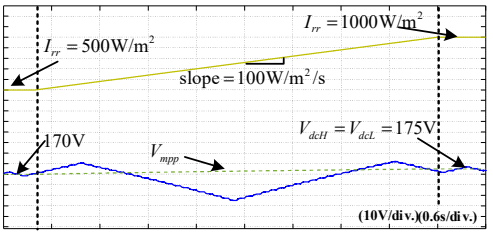

(a)

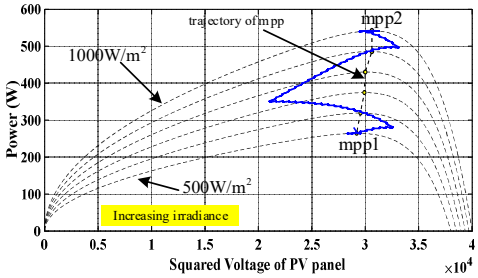

(b)

Fig. 17. Simulation results with the P-V^2 curve-based MPPT using P&O algorithm under same dynamic irradiance condition of Fig. 16. (a) Transient response and convergence behavior. (b) Trajectory on the P-V^2curve.

As an example of unstable MPPT, the PI gains in the dc-link voltage control loop are changed such that the new transfer functions become

$$G_{dc}(s) = \frac{0.003664s + 0.06609}{8.2\times10^{-7}s^3 + 820\times10^{-6}s^2 + 0.003664s + 0.06609}$$

$$G(s) = \frac{-(3.664s^2 + 886.9s + 14800)}{8.2\times10^{-7}s^4 + 820\times10^{-6}s^3 + 0.003664s^2 + 0.06609s},$$

and the corresponding Nyquist plots are shown in Fig. 18(b). The PI gains of the MPPT are increased from the case 1 to 4, and it is observed that the Nyquist plots do not satisfy the criterion (10) for high PI gains. Therefore, the stability cannot be guaranteed anymore. As theoretically expected, when the stability condition (10) is violated the MPPT becomes more and more unstable as can be seen from the dc-link voltage waveforms in the simulation results of the cases 2-4 in Fig. 18(a). Therefore, the stability criterion (10) serves as a good guideline to guarantee the stability of the proposed P-V^2 based MPPT.

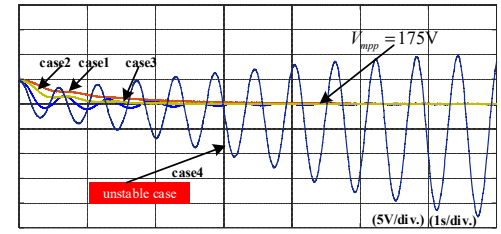

(a)

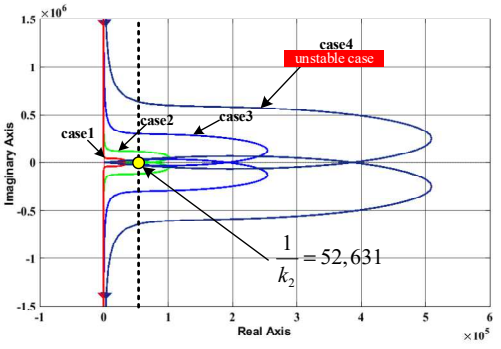

(b)

Fig. 18. Simulation results with the proposed P-V^2 curve-based MPPT using feedback control under various PI gains of the MPPT. (a) dc-link (panel) voltage transient response. (b) corresponding Nyquist plots of $G(s)$.

VI. Conclusion

To increase the tracking speed of the MPPT without facing instability issue, this paper presents a new P-V^2 curve-based maximum power point tracking algorithm which adopts the squared voltage of the PV panel as the control variable. Together with the dc-link voltage control with the squared voltage as the command, the whole MPPT system conforms to the Lure's system structure. The closed-loop stability is then rigorously analyzed to obtain design guidelines for stable MPPT using the circle criterion. It is confirmed that so long as the dc-link voltage control loop and the MPPT feedback controller is designed to satisfy the stability condition, the response time of the proposed P-V^2 based MPPT can be much shorter than the conventional P&O MPPT method while its stability is guaranteed. The static and dynamic performance of the proposed MPPT is also improved. The correctness of the analytical results and the effectiveness of the proposed MPPT method are finally verified by simulation on Matlab/Simulink.

References

[1] M. A. Danandeh and S. M. Mousavi G., "Comparative and comprehensive review of maximum power point tracking methods for PV cells," *Renewable and Sustainable Energy Reviews.*, vol. 82, pp. 2743-2767, Feb. 2018.

[2] T. Esram, and P. L. Chapman, "Comparison of Photovoltaic Array Maximum Power Point Tracking Techniques," *IEEE Trans. Energy conversion*, vol. 22, no. 2, pp. 439-449, June 2007.

[3] M. A. Elgendy, B. Zahawi and D. J. Atkinson, "Assessment of Perturb and Observe MPPT Algorithm Implementation Techniques for PV Pumping Applications," *IEEE Trans. Sustain. Energy*, vol. 3, no. 1, pp. 21-33, Jan. 2012.

[4] M. A. Elgendy, B. Zahawi and D. J. Atkinson, "Assessment of the Incremental Conductance Maximum Power Point Tracking Algorithm," *IEEE Trans. Sustain. Energy*, vol. 4, no. 1, pp. 108-117, Jan. 2013.

[5] O. Wasynezuk, "Dynamic Behavior of a Class of Photovoltaic Power Systems, " *IEEE Trans. Power Apparatus and Systems*, vol. PAS-102, no. 9, pp. 3031-3037, Sept. 1983.

[6] K. Harada and G. Zhao, "Controlled power interface between solar cells and AC source," *IEEE Trans. Power Electron.*, vol. 8, no. 4, pp. 654-662, Oct. 1993.

[7] K. H. Hussein, I. Muta, T. Hoshino, and M. Osakada, "Maximum Photovoltaic power tracking: An algorithm for rapidly changing atmospheric conditions," *Proc. Inst. Elect. Eng., Gener., Transmiss., Distrib.,* vol. 142, no. 1, pp. 59–64, Jan. 1995.

[8] F. Liu, S. Duan, F. Liu, B. Liu and Y. Kang, "A Variable Step Size INC MPPT Method for PV Systems," *IEEE Trans. Ind. Electron.*, vol. 55, no. 7, pp. 2622-2628, July 2008.

[9] S. J. Chiang, K. T. Chang and C. Y. Yen, "Residential photovoltaic energy storage system," *IEEE Trans. Ind. Electron.*, vol. 45, no. 3, pp. 385-394, June 1998.

[10] H. Sugimoto and H. Dong, "A new scheme for maximum photovoltaic power tracking control," *Proceedings of Power Conversion Conference - PCC '97*, 1997.

[11] D. Sera, L. Mathe, T. Kerekes, S. V. Spataru and R. Teodorescu, "On the Perturb-and-Observe and Incremental Conductance MPPT Methods for PV Systems," *IEEE Journal of Photovoltaics*, vol. 3, no. 3, pp. 1070-1078, July 2013.

[12] T. Kouno, "Maximum power obtainable in a nonlinear system," in *Proceedings of the IEEE*, vol. 66, no. 9, pp. 1085-1086, 1978.

[13] B. Jayawardhana, H. Logemann and E. P. Ryan, "The Circle Criterion and Input-to-State Stability," *IEEE Control Systems Magazine*, vol. 31, no. 4, pp. 32-67, Aug. 2011.

[14] E. I. Batzelis, G. Anagnostou, I. R. Cole, T. R. Betts and B. C. Pal, "A State-Space Dynamic Model for Photovoltaic Systems With Full Ancillary Services Support," *IEEE Trans. Sustain. Energy*, vol. 10, no. 3, pp. 1399-1409, July 2019.

[15] M. Ariyapuek, S. Suwankawin, S. Sangwongwanich and A. Sangwongwanich, "Double-Carrier-Based PWM Theory for Independent Power Control of Dual-Input Three-level Inverters," *Proc. IPEC.*, pp. 940-944, May 2022.